RSC Advances

ROYAL SOCIETY OF CHEMISTRY

www.rsc.org/advances

Axial Ligand Modified High Valent Tin(IV) Porphyrins: Synthesis, Structure, Photophysical Studies and Photodynamic Antimicrobial Activities on Candida Albicans

Rahul Soman[a], Darpan Raghav[b], Subramaniam Sujatha[a], Krishnan Rathinasamy[b] and Chellaiah Arunkumar[a*]*

The photophysical studies, fluorescence imaging, single crystal x-ray structure analysis and DFT calculations revealed that the compounds **2** and **3** have shown enhanced phototoxicity towards *Candida albicans* compared to **1**.

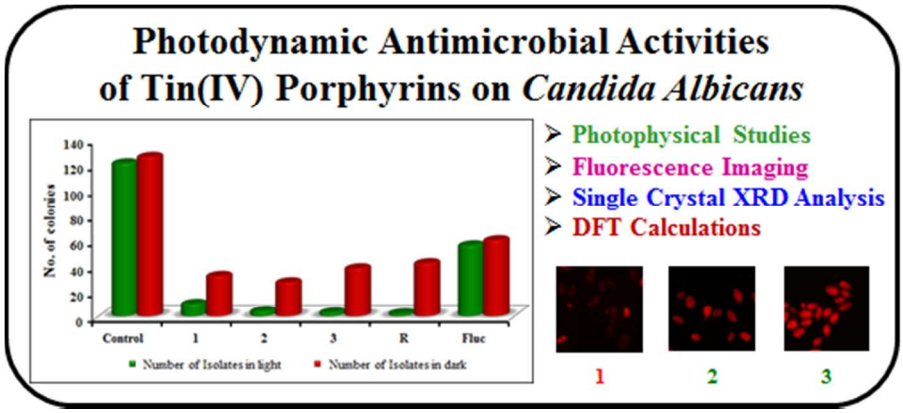

Axial Ligand Modified High Valent Tin(IV) Porphyrins: Synthesis, Structure, Photophysical Studies and Photodynamic Antimicrobial Activities on Candida Albicans

Rahul Soman[a], Darpan Raghav[b], Subramaniam Sujatha[a], Krishnan Rathinasamy[b*] and Chellaiah Arunkumar[a*]

Herein, we report the synthesis, structure, photophysical properties and photodynamic antimicrobial activities on *Candida albicans* using axial ligand modified high valent tin(IV) porphyrins, namely $Sn^{IV}(OH)_2T(4\text{-}CMP)P$ (**1**), $Sn^{IV}(OH)_2T(4\text{-}CP)P$ (**2**) and $Sn^{IV}(O\text{-}NO_2Ph)_2T(4\text{-}CMP)P$ (**3**). The newly synthesized porphyrins were characterized by various spectroscopic methods and single crystal X-ray diffraction analysis. The crystal structure analysis of precursor porphyrin, $Sn^{IV}(Cl)_2T(4\text{-}CMP)P$ and **3** are well stabilized by various intermolecular interactions and porphyrin **3** shows complementary bonding interactions between the nitro groups (N···O) forming one dimensional array. The fluorescent lifetime of **3** is less compared to other porphyrins which indicates that there is a considerable interaction between the tin(IV) porphyrin core and nitrophenyl system and this could be the reason for its significant phototoxicity. This is further evident from X-ray crystallography and DFT calculations. In the presence of light, tin(IV) porphyrins significantly inhibited the growth of *C. albicans* in liquid as well as in the solid agar medium and the growth inhibitory effects were very less under dark conditions. The porphyrin internalisation as well as localization within the *Candida* cells was examined by fluorescence microscopic analysis. Our results suggest that the mechanism behind the photodynamic inactivation of *C. albicans* could be through the generation of singlet oxygen species within the cells.

Introduction

Photodynamic antimicrobial chemotherapy[1] (PACT), a new treatment modality, follows similar principles as that of photodynamic therapy (PDT) that utilizes nontoxic components such as light, oxygen and a photosensitizing agent, promoting microbial eradication by the production of reactive oxygen species such as singlet oxygen, superoxide and hydroxyl radicals.[2] Photosensitizer is generally allowed to get internalized within the prokaryotic or eukaryotic cells of interest. When the cells containing photosensitizers are exposed to light of a specific wavelength, it gets excited to singlet excited state and undergoes intersystem crossing, reaches triplet energy state. While coming back to its ground state, the photosensitizer produces singlet oxygen from cellular oxygen, which causes cell damage leading to cell death.[2] (Scheme 1a)

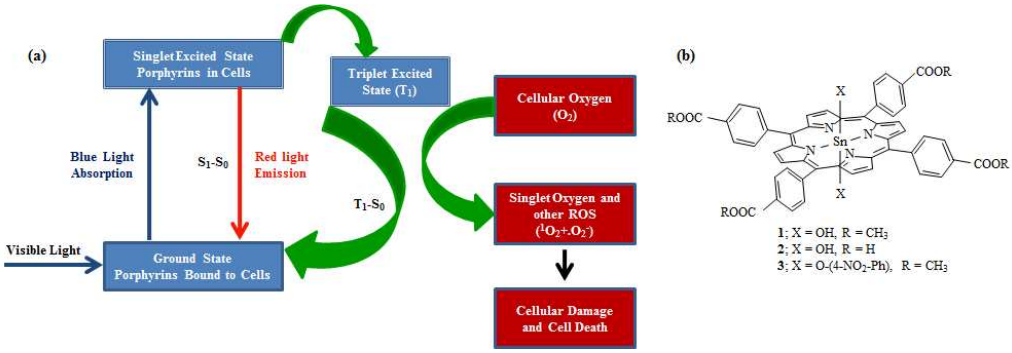

Scheme. 1 (a) Mechanism for the photodynamic antimicrobial chemotherapy; (b) Schematic representation of tin(IV) porphyrins, **1**–**3** in this study.

Porphyrin based photosensitizers are widely accepted because it shows promising broad spectrum of activity against microorganisms.[3] *C. albicans* is an opportunistic fungal pathogen which can affect vital areas of the body and its infections are more frequent in immunocompromised individuals.[4] Such severe infections are difficult to treat and were usually cured with azoles which target the fungal cell membranes.[5] However, there is a growing interest towards finding better alternatives to treat infections caused by *C. albicans* as these are developing resistance towards established azoles.[6] The ability of photosensitizers to cause photodynamic damage depends on their photophysical properties. A good photosensitizer preferably has high triplet state quantum yields and long triplet state lifetimes.[7] Recently, tin(IV) porphyrins have shown much attention owing to their interesting photophysical properties.[8] They are very stable, ease of synthesis, diamagnetic and usually six-coordinated with *trans*-diaxial ligands.[9] High valent tin(IV) porphyrins with chlorine as

its axial ligands such as tin(IV) ethyl etiopurpurin and tin(IV) octaethylbenzochlorin were the two well established second-generation photosensitizers.[10] In this line, we are inspired to explore the synthesis, structure and photophysical properties of axial ligand modified tin(IV) porphyrins (**1**–**3**) (Scheme 1b) with hydroxyl and 4-nitrophenolate moieties. To better understand the electronic transitions that takes place in $Sn^{IV}(Cl)_2T(4\text{-CMP})P$, **1** and **3**, computational studies were performed. The photodynamic antimicrobial chemotherapy of *C. albicans* using the porphyrins, **1**–**3** were also studied. The cytotoxic effects of porphyrins were assessed in *C. albicans* cells by agar well diffusion and broth assay. Microscopic analysis and antifungal assays were done in order to confirm the internalization of compounds as well as for demonstrating the phototoxicity induced by these compounds in *C. albicans*.

Experimental

Materials and methods

Chemicals employed for the synthesis were obtained as AR grade and used as received. Solvents were purified using the available literature methods.[11] The reference compound, *meso*-tetrakis(4-N-methylpyridyl)porphyrin, **R** [$H_2T(4\text{-NMP})P$] was prepared according to the literature procedure.[12] Chemicals used for antimicrobial studies were purchased from HiMedia and Sigma Aldrich. Optical absorption spectra were recorded at room temperature on Shimadzu UV-2450 spectrophotometer and ^1H NMR spectra were taken using a Bruker Avance III 400 MHz spectrometer. Fluorescence spectra and quantum yield measurements were performed using a Perkin Elmer LS 55 luminescence spectrophotometer at 25.0 ± 0.5 °C. Fluorescence lifetime measurements were calculated from time-resolved fluorescence intensity decays using a Horiba Scientific Fluoromax-4 spectrofluorometer with data station software in time correlated single photon counting mode. A pulsed light-emitting diode (Horiba NanoLED-560) was used as an excitation source. This LED generates optical pulse at 564 nm of pulse duration 1.5 ns. LED profile (instrument response function) was measured at the excitation wavelength using a Ludox 530 (colloidal silica) as the scatterer. To optimize the signal-to-noise ratio, 10000 photon counts were collected in the peak channel. Photo-irradiations were done using a General electric Quartz line lamp (300 W). Light intensities were measured with a pyroelectric detector (RJP-735 from Laser Probe) which is connected

to an energy ratio meter (RJ-7620 from laser probe). The study was conducted for an irradiation time of 300 min and the average light fluence rate was 95 μJ/cm^2).

Synthesis of tin(IV) porphyrins

Synthesis of *trans*-dihydroxy[5,10,15,20-tetrakis(4'-carboxymethylphenyl) porphyrinato] tin(IV), $Sn^{IV}(OH)_2T(4\text{-}CMP)P$, 1

The precursor, 5,10,15,20-tetrakis(4'-carboxymethylphenyl)porphyrin [$H_2T(4\text{-}CMP)P$] was synthesized using modified Lindsey method[13] and the crude product was purified by silica gel column chromatography using acetone / chloroform as eluent. Evaporation of the solvent and recrystallization from chloroform / hexane results the desired product with 40 % yield. UV-Visible data in THF, λ_{max} (log ε / M^{-1} cm^{-1}): 417 (6.12), 514 (4.88), 549 (4.50), 591 (4.33), 646 (4.12). ^{1}H NMR data in $CDCl_3$ (δ in ppm) (400 MHz): 8.82 (s, 8H, β-pyrrole-H), 8.44–8.46 (d, 8H, J = 8.00 Hz, *o*-phenyl-H), 8.28–8.31 (d, 8H, J = 8.00 Hz, *m*-phenyl-H), 4.11 (s, 12H, *p*-carboxymethyl-H), −2.81 (s, 2H, imino-H).

Tin metallation was performed as per the reported method[14] using stannous chloride as metal ion carrier in pyridine. Excess water was added to precipitate the product which was then filtered. The crude product was re-dissolved in chloroform, passed through anhydrous Na_2SO_4 and purified using neutral alumina in chloroform / acetone mixture. The unreacted free base porphyrin was collected initially, after which *trans*-dichloro[5,10,15,20-tetrakis(4'-carboxymethylphenyl) porphyrinato] tin(IV), $[Sn^{IV}(Cl)_2T(4\text{-}CMP)P]$ was separated out from the column. The solvent was evaporated to dryness under vacuum and the yield was noted as 80 %. ^{1}H NMR data in $CDCl_3$ (δ in ppm) (400 MHz): 9.19 (s, 8H, β-pyrrole-H), 8.51–8.53 (d, 8H, J = 8.00 Hz, *o*-phenyl-H), 8.40–8.42 (d, 8H, J = 8.00 Hz, *m*-phenyl-H), 4.13 (s, 12H, *p*-carboxymethyl-H). This product was re-dissolved in tetrahydrofuran and reacted with slight excess of potassium carbonate (1:50) in minimum quantity of water for 6 hrs. After evaporation of solvent, the residue was re-dissolved in acetone / chloroform mixture and then passed through anhydrous Na_2SO_4. It was then purified using neutral alumina to give **1** and the yield was found to be 75 %. UV-Visible data: λ_{max} (log ε / M^{-1} cm^{-1}), (a) in THF: 427 (5.97), 561 (4.89), 600 (4.76); (b) in acetone: 423 (5.86), 555 (4.47), 595 (4.20). ^{1}H NMR data in $CDCl_3$ (δ in ppm) (400 MHz): 9.10 (s, 8H, β-pyrrole-H), 8.50–8.52 (d, 8H, J = 8.00 Hz, *o*-phenyl-H), 8.41–8.43 (d, 8H, J = 8.00 Hz, *m*-phenyl-H), 4.11 (s, 12H, *p*-carboxymethyl-H).

Synthesis of *trans*-dihydroxy[5,10,15,20-tetrakis(4'-carboxyphenyl)porphyrinato] tin(IV), $Sn^{IV}(OH)_2T(4\text{-}CP)P$, 2

To the THF solution of **1**, potassium hydroxide (20 equiv.) was added and the resultant solution was refluxed for 24 hrs. The precipitated product was filtered to get the purple solid residue and further treated with 0.01 N HCl (Caution: If the acid concentration is slight excess, demetallation occurs) to obtain the final product. The porphyrin layer was extracted with ethyl acetate, dried under vacuum and the yield was 60 %. UV-Visible data: λ_{max} (log ε / M^{-1} cm^{-1}), (a) in THF: 430 (5.84), 563 (4.69), 602 (4.18); (b) in acetone: 425 (5.14), 561 (3.97), 601 (3.87). ^{1}H NMR data for **2** in DMSO-d6 (δ in ppm) (400 MHz): 9.32 (s, 8H, β-pyrrole-H), 8.47–8.49 (d, 8H, J = 8.00 Hz, *o*-phenyl-H), 8.44–8.46 (d, 8H, J = 8.00 Hz, *m*-phenyl-H). ESI-mass data of **2**: 939 $[M\text{-}2H]^+$ (Calcd. 941).

Synthesis of *trans*-dinitrophenolate [5,10,15,20-tetrakis(4'-carboxymethylphenyl) porphyrinato] tin(IV), $Sn^{IV}(O\text{-}NO_2Ph)_2T(4\text{-}CMP)P$, 3

Porphyrin, **1** and 4-nitrophenol in nitrobenzene was magnetically stirred at 100–120 °C for 4 hrs. The formed porphyrin phenolate complex was crystallized using hexane to afford dark red single crystals of **3** after a week time. UV-Visible data: λ_{max} (log ε / M^{-1} cm^{-1}), (a) in THF: 425 (5.84), 558 (4.73), 597 (4.29); (b) in acetone: 421 (6.17), 553 (4.84), 592 (4.58). ^{1}H NMR data for **3** in $CDCl_3$ (δ in ppm) (400 MHz): 9.06 (s, 8H, β-pyrrole-H), 8.45–8.47 (d, 8H, J = 8.00 Hz, *o*-carboxymethylphenyl-H), 8.14–8.16 (d, 8H, J = 8.00 Hz, *m*-carboxymethylphenyl-H), 6.54–6.55 (d, 8H, J = 7.20 Hz, *m*-nitrophenyl-H), 4.07 (s, 12H, *p*-carboxymethyl-H), 1.74–1.76 (d, 8H, J = 7.20 Hz, *o*-nitrophenyl-H).

Crystal structure determination

X-ray quality single crystals of compounds, $Sn^{IV}(Cl)_2T(4\text{-}CMP)P$ and **3** were obtained by slow vapour diffusion method using chloroform / hexane and nitrobenzene / hexane respectively. Red crystals were mounted on a glass capillary with suitable size and the crystal data was collected on a Bruker AXS Kappa Apex II CCD diffractometer with graphite mono-chromated Mo K_α radiation (λ = 0.71073 Å) at 298 K. The reflections with $I > 2\sigma(I)$ were employed for structure solution and refinement. The SIR92[15] (WINGX32) program was used for solving the structure by direct methods. Successive Fourier synthesis was employed to complete the structures after full-matrix least squares refinement on $|F|^2$ using the SHELXL97[16] software.

Hirshfeld surface analysis

To analyse and quantify the various intermolecular interactions present in the crystal structure of tin(IV) porphyrins, we have generated the Hirshfeld surfaces and 2D fingerprint plots using *Crystal Explorer 3.1*.[17]

Microorganism and growth conditions

C. albicans strain CAF4-2 was obtained from Molecular genetics laboratory, School of Biotechnology, National Institute of Technology Calicut. The organism was grown aerobically at 37 °C in a standard YPD medium containing 1 % yeast extract, 2 % peptone, 2 % dextrose[18]. Since the strain is ura^-, the growth medium was supplemented with 25 μg/mL uridine.[19]

Agar well diffusion assay for determining the photodynamic growth inhibition of *C. albicans*

YPD Broth and YPD agar supplemented with uridine were prepared and sterilized by autoclaving. *C. albicans* was initially grown overnight in 5 mL YPD Broth in a shaking incubator. Shaking was maintained at 200 rotations per minute (rpm) while the temperature was kept constant at 37 ^oC. YPD Agar containing petri plates were prepared by pouring the sterile YPD Agar into sterile petri plates to a uniform depth of 4 mm which is equivalent to approximately 25 mL in a 90 mm plate. The medium was allowed to solidify in the plates and the overnight culture of *C. albicans* was spread evenly on the top of the solidified agar with the help of a sterile cotton swab. Wells were made in the agar plates for addition of the porphyrin solutions. Three different concentrations of all the porphyrins were added in equal volumes. The organism was allowed to grow aerobically at 37 ^oC in light or dark conditions. After 12 hrs of incubation, the zone of inhibition was calculated by using the formula given below:[20]

$$\% \text{ of inhibition} = \frac{\text{I (Diameter of the inhibition zone in mm x 100)}}{\text{90 (Diameter of the Petri-plate in mm)}}$$

Photodynamic inactivation of *C. albicans* in broth assay: Determination of half maximal inhibitory concentration (IC_{50}) and minimum inhibitory concentration (MIC) values of porphyrins

The *C. albicans* cells were inoculated in YPD liquid medium containing different concentrations of porphyrins or 0.2 % DMSO (solvent control). The growth inhibition of *C. albicans* was studied by monitoring absorbance at 600 nm *(A600)*, at different time intervals (0, 15, 30, 60, 90, 120, 150, 180, 240 and 300 min) in the presence of 3 different concentrations of all the compounds (10, 25 and 50 μM) and 20 μg/mL of fluconazole as a positive control. A comparative study of the same was done by varying the experimental conditions in light and dark. The A600 value of control where no compound was added was subtracted with A600 value obtained after adding the compound. The same was followed in all the cases where compounds were added. The percentage inhibition of *Candida* growth was calculated by using the equation:[21]

$$\% \text{ of inhibition} = [1-(X_{A600} / C_{A600})] \times 100$$

where, X_{A600} represents the *A*600 value of *X* μM compound treated culture at the different time points. C_{A600} represents the *A*600 of the control culture at the same time. The percentage of growth inhibition was determined for 5 hrs after the addition of porphyrins to the *C. albicans* culture. The IC_{50} values of compounds were determined by plotting the percentage inhibition of cell growth against compound concentration.[21]

C. albicans cells were grown for 4 hrs in the absence and presence of the compounds in light and dark conditions. The lowest concentration of the compound that inhibited the visible growth of the *C. albicans* was considered as the MIC. The concentration of the compound, in which there was no visible growth was diluted and spread on to the agar plates and incubated for additional 12 hrs at 37 ℃. The number of colony-forming units was calculated by counting the colonies on each plate.[21]

Cellular uptake profiling of porphyrins in *C. albicans* cells

In order to establish a time profile for intracellular accumulation of the compounds, a spectrofluorimetric analysis was carried out. *C. albicans* cells treated with different porphyrins were allowed to grow in 5 mL liquid culture. The cultures were incubated in a shaking incubator in the dark. After 30, 60, 90, 120, 150, 180, 240 and 300 minutes, aliquots

of cells were harvested by centrifuging at 6000 rpm for 5 minutes. The supernatant liquid was discarded and the cell pellet was washed thrice with 1 mL of 1X PBS in order to remove the uninternalized porphyrins. After this, cells were gently resuspended in 1X PBS and then were transferred into 1 mL fluorescence cuvette. A fluorescence spectral analysis was carried out by exciting the samples at 550 nm.[22]

Wide field fluorescence microscopic analysis

For studying the intracellular localization and phototoxicity of the compounds, two sets of *C. albicans* cells were grown in liquid medium. One set of cells were cultured and grown by incubating in dark for 6 hrs. Another set was initially grown in the dark for 6 hrs and was then exposed to light and grown for 3 more hrs. The cells were then harvested and washed thrice with 1X PBS in order to remove the excess un-internalised compounds. As per the spectrofluorimetric analysis, the porphyrins get excited around 550 nm and give emission around 600 nm. Hence, for this study the compounds were excited using the green filter (490-510 nm). *C. albicans* cells were stained with Hoechst 33342 (10 μg/mL followed by 30 minutes incubation) to visualize the DNA[23]. The fluorescence imaging was performed using LEICA DM5000B fluorescent microscope (Germany) at 100x magnification (oil immersion) and the images were processed by using ImageJ (NIH, USA).

Confocal fluorescence microscopic studies

The *C. albicans* cells grown in YPD medium as described above were incubated in dark with the compounds for 6 hrs. The cells were then harvested and washed thrice with 1X PBS in order to remove the excess un-internalised compounds. Cells were then mounted on clean glass slides and sealed for microscopic analysis.[24] The confocal fluorescence imaging was performed using Confocal fluorescent microscope (Germany) at 63x magnification. To confirm the internalization of the compounds, a progressive confocal optical slicing approach was employed. Images were sliced progressively at every 0.8 μm depth and the internalization of the compounds was analysed. Images were obtained by merging bright field and fluorescent images and further processed by using ImageJ (NIH, USA).

Measurement of singlet oxygen

1,3-Diphenylisobenzofuran (DPBF) was used as a selective singlet oxygen ($^1O_2$) acceptor, which was bleached upon reaction with $^1O_2$ generated by porphyrin donors. DPBF (1.7 x 10^{-7} M) solutions without or with porphyrin derivatives (6.6 x 10^{-7} M) were prepared in DMSO under dark conditions. These solutions were irradiated at room temperature and under gentle magnetic stirring. The breakdown of DPBF was monitored by measuring the decrease in absorbance at 410 nm at pre-established irradiation intervals.[25] From this plot, the rates of $^1O_2$ production of porphyrins **1**–**3** relative to those of H_2TPP and **R** were determined.

Results and Discussion

Synthesis

The precursor, H_2T(4-CMP)P was prepared using the modified procedure of Lindsey *et al.*[13] and their tin(IV) complexes, $Sn^{IV}(Cl)_2$T(4-CMP)P, **1** and **2** were prepared by the variant literature methods.[14] Synthesis of **3** was done by condensing **1** with 4-nitrophenol (Scheme 2). Synthesized porphyrins were isolated, purified by column chromatography and characterized by UV-Visible, ^{1}H NMR spectroscopic methods, mass spectrometry and single crystal X-ray diffraction analysis.

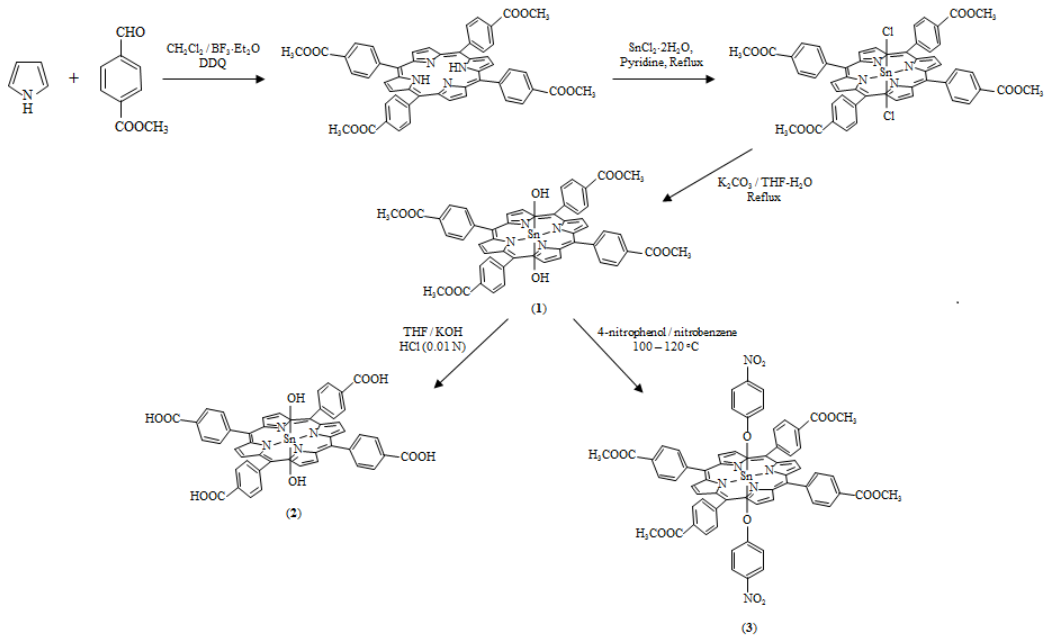

Scheme 2. General synthesis of tin(IV) porphyrins, **1**–**3**.

Photophysical properties

The photophysical properties such as optical absorption, steady state emission, fluorescence quantum yield and fluorescence decay profile were studied for tin(IV) porphyrins **1**–**3**, $Sn^{IV}(OH)_2TPP$ and the porphyrin ligand $H_2T(4\text{-CMP})P$ in THF medium. The electronic absorption spectra of tin(IV) porphyrins exhibit an intense Soret (B) band corresponds to $S_0 \rightarrow S_2$ transition around 425 nm and two visible (Q) bands around 560 and 600 nm which corresponds to $Q_{(1,0)}$ and $Q_{(0,0)}$ peaks of $S_0 \rightarrow S_1$ transition.[26] It is observed that there is a marginal red shifted absorption spectrum for **2** and a marginal blue shifted absorption spectrum for **3** compared to that of **1** in THF as well as acetone media (Fig. S1). The steady-state fluorescence of porphyrins was performed in order to study their electronic properties in excited state. The normalized absorption and emission spectrum of porphyrin **3** is shown in Fig. 1.

On excitation near the Soret band, all the tin(IV) porphyrins exhibit two well-defined emission bands near 605 nm (band 1) and 657 nm (band 2) which corresponds to $S_1 \rightarrow S_0$ transition and the spectral profile is comparable with the reported hexa-coordinated tin(IV) porphyrin systems.[9,26] Also, there is a very weak emission corresponding to $S_2 \rightarrow S_0$ transition at 434, 462 and 489 nm for porphyrins, $Sn^{IV}(OH)_2TPP$, **1** and **2** respectively (Table 1).

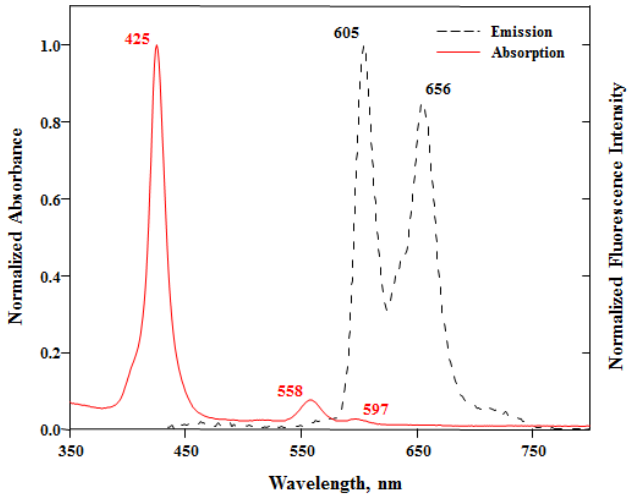

Fig. 1 Normalized absorption (solid line) and emission (dashed line) spectra of **3** in THF at 298 K. Emission spectra was recorded by exciting the Soret region.

Table 1 Photophysical data of porphyrins recorded in tetrahydrofuran at 300 K.

Porphyrin	Absorption λ_{max} (nm)	Fluorescence[a] λ_{max} (nm)	Quantum Yield $\Phi_f(S_1\text{-}S_0)$	Fluorescence lifetime, τ (ns)
$H_2T(4\text{-CMP})P$	417, 514, 549, 591, 646	650, 716	0.057	10.10[b]
$Sn^{IV}(OH)_2TPP$	425, 560, 600	434, 604, 656	0.044	01.48[c]
1, $Sn^{IV}(OH)_2T(4\text{-CMP})P$	427, 561 600	462, 605, 657	0.017	01.75[d]
2, $Sn^{IV}(OH)_2T(4\text{-CP})P$	430, 563, 602	489, 605, 658	0.008	0.90[d]
3, $Sn^{IV}(O\text{-}NO_2Ph)_2T(4\text{-CMP})P$	425, 558, 597	605, 656	0.010	0.66[d]

[a]Fluorescence spectra of porphyrins were obtained as a function of λ_{ex} in the Soret band region. [b]Excited at 460 nm and emission monitored at 650 nm in toluene. [c]Excited at 460 nm and emission monitored at 600 nm in toluene. [d]Excited at 460 nm and emission monitored at 600 nm in DMF.

The $S_1 \rightarrow S_0$ fluorescence quantum yield (Φ_f) of the tin(IV) porphyrins were also measured using H_2TPP as the reference[27] ($\Phi_f = 0.11$). As seen from the data given in table 1, there is a quenching of fluorescence in **2** and **3** compared to **1** which may be due to the excited state processes such as enhanced internal conversion, intersystem crossing etc.[26] As anticipated, the metalloporphyrins show low quantum yields compared to the free ligand, $H_2T(4\text{-CMP})P$ which indicates that the metal coordination may induce the radiationless decay rate.[28] The fluorescence decay profiles (λ_{exc} = 460 nm and λ_{em} = 600 nm) of porphyrins measured by time-correlated single photon counting (TCSPC) technique shown that the fluorescent life time for **3** is shorter than that of **1** which supports that the tin(IV) porphyrin and nitrophenyl system considerably interact with each other (Fig. 2).[29] This is further confirmed by the crystal structure analysis of **3** (Fig. 4b) which indicates that there is an π–π interaction between porphyrin plane and 4-nitrophenyl system due to their close proximity. The fluorescence decay times were summarized in table 1 and the S_1 lifetimes (τ) of porphyrins, **1**–**3** were determined to be 1.75, 0.90 and 0.66 ns respectively. The τ of porphyrin **2** is comparable with the reported tin(IV) porphyrin, $Sn^{IV}(OH)_2THP$ and its value is 0.91 ns.[30]

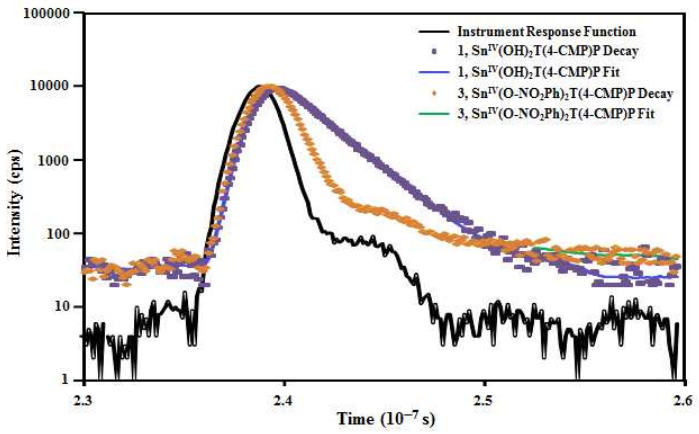

Fig. 2 Fluorescence decay curves of **1** and **3** observed at 600 nm along with IRF measured in THF. (λ_{exc} = 460 nm)

Crystal structure description of porphyrins, $Sn^{IV}(Cl)_2T(4\text{-}CMP)P$ and 3

Single crystal XRD analysis showed that the porphyrins, $Sn^{IV}(Cl)_2T(4\text{-}CMP)P$ and **3** crystallized in triclinic P-1 system (Table 2). The asymmetric unit of $Sn^{IV}(Cl)_2T(4\text{-}CMP)P$ consists half a molecule of porphyrin and an acetonitrile molecule in which the porphyrin plane is found to be almost planar in nature. The ORTEP and molecular crystal packing diagrams of $Sn^{IV}(Cl)_2T(4\text{-}CMP)P$ are shown in Fig. 3. The solvent molecule (CH_3CN) acts as a bridge connecting two neighbouring porphyrin molecules through strong hydrogen bonding between nitrogen of the acetonitrile with the *β*-pyrrole hydrogen [$_{(Solvent)}N\cdots H_{(\beta\text{-pyrrole})}$, 2.733 Å] of one molecule and with phenyl-hydrogen [$_{(Solvent)}N\cdots H_{(phenyl)}$, 2.631 Å] of the another molecule which is viewed along 'bc' plane and depicted in Fig. 3b. Other intermolecular interactions which makes the compound $Sn^{IV}(Cl)_2T(4\text{-}CMP)P$ to form the two dimensional array of molecules viewed down 'ab' plane (Fig. 3c) involving Sn-Cl$\cdots C_{(\beta\text{-pyrrole})}$ (3.368 Å) and O$\cdots$H bonding [$_{(carbonyl)}O\cdots H_{(\beta\text{-pyrrole})}$, 2.421 Å and $_{(carbonyl)}O\cdots H_{(carboxymethyl)}$, 2.634 Å]. Overall, the crystal structure of $Sn^{IV}(Cl)_2T(4\text{-}CMP)P$ is well stabilized by various intermolecular interactions described above.

Fig. 4a and 4b represents the top and side-on view of ORTEP diagrams of **3** respectively. From the side-on view, it is clear that the porphyrin core is planar and the two axial ligands (4-nitrophenyl ring) are present in the apex positions which make an angle of 123.18 (14)^o between the porphyrin mean plane and 4-nitrophenyl ring through oxygen atom of the phenolate.

Table 2 Summary of crystal structure data of porphyrins.

	$Sn^{IV}Cl_2T(4\text{-}CMP)P$	**3**
Formula	$C_{56}H_{42}Cl_2N_6O_8Sn$	$C_{64}H_{44}N_6O_{14}Sn$
Formula weight	1116.55	1239.74
CCDC	948482	974215
Crystal System	Triclinic	Triclinic
Space Group	P-1	P-1
Density, mg/m^3	1.468	1.276
a [Å]	7.8170(3)	10.6568(5)
b [Å]	10.9187(4)	12.5048(5)
c [Å]	15.3971(6)	13.3413(5)
α [deg]	93.089(2)	73.218(3)
β [deg]	99.167(2)	76.096(4)
γ [deg]	102.119(2)	74.284(4)
V [$Å^3$]	1263.26(8)	1612.99(12)
λ, Å	0.71073	0.71073
Z	1	1
Temperature, K	293(2)	293(2)
No. of unique reflections	4958	6337
GOF on F^2	1.081	1.099
R_1[a]	0.0288	0.0349
wR_2[b]	0.0778	0.0865

[a]$R_1 = \Sigma||F_o|-|Fc||/\Sigma|F_o|$; $I_o > 2\sigma(I_o)$. [b]$wR_2 = [\Sigma\, w(F_o^2-F_c^2)^2/\Sigma w(F_o^2)^2]^{1/2}$.

Fig. 4c represents the three dimensional network arrangement of **3** (viewed down 'a' axis) depicting various intermolecular interactions, viz., $_{(carbonyl)}O\cdots H_{(carboxymethyl)}$, 2.582 Å, $_{(carbonyl)}O\cdots H_{(phenyl)}$, 2.384 Å, $_{(nitro)}O\cdots H_{(\beta\text{-pyrrole})}$, 2.587 Å, $_{(\beta\text{-pyrrole})}C\cdots H_{(phenyl)}$, 2.759 – 2.884 Å, $_{(\beta\text{-pyrrole / phenyl})}C\cdots H_{(carboxymethyl)}$, 2.885 Å, $_{(nitro)}N\cdots O_{(nitro)}$, 3.002 Å and each interactions are present in the asymmetric unit of **3** in two numbers. Interestingly, the nitro group present in the apex positions are involving complementary bonding interactions between the nitrogen of one molecule with the oxygen of another molecule making a one dimensional array of molecules (Fig. 4d).

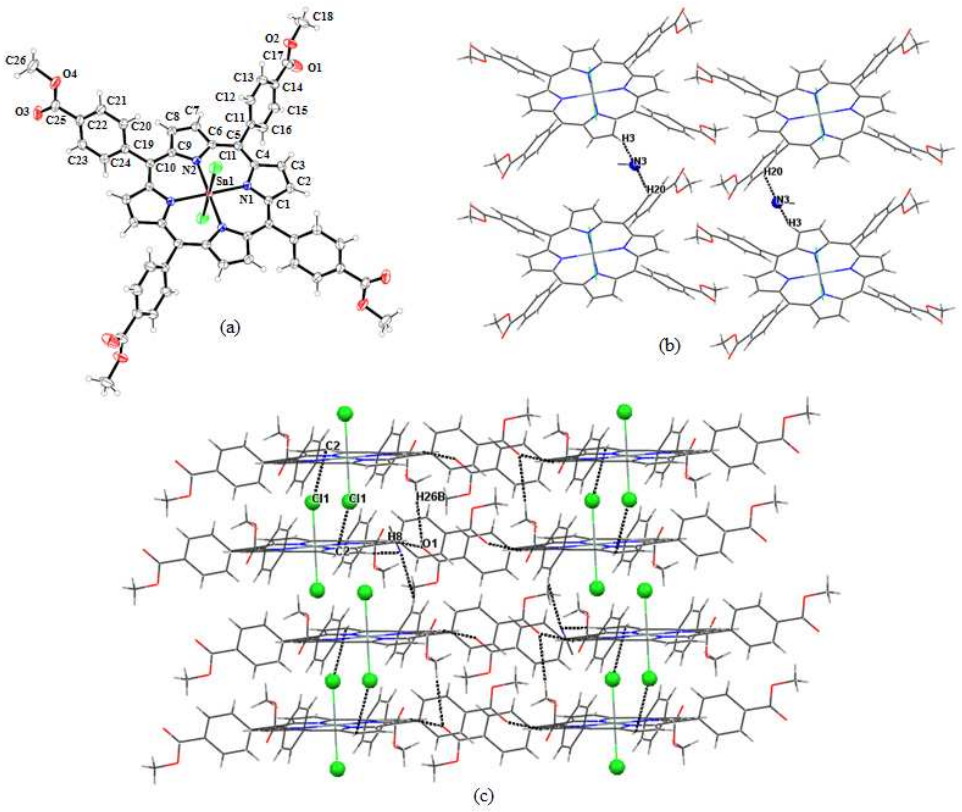

Fig. 3 (a) ORTEP diagram of $Sn^{IV}(Cl)_2T(4\text{-CMP})P$ with atomic numbering (solvent molecule, acetonitrile is not shown for clarity; thermal ellipsoids shown at 40 % probability level); Molecular crystal packing diagram of $Sn^{IV}(Cl)_2T(4\text{-CMP})P$ (b) depicting N···H bonding viewed along 'bc' plane; (c) depicting Cl···C and O···H bonding viewed down 'ab' plane.

The Sn^{IV}–O bond length in **3** is compared with various tin(IV) porphyrins available in the literature[31-33] and the data are presented in table 3. It is seen that the observed bond length in **3** (2.066 Å) is comparable with the tin(IV) porphyrins containing phenolic BODIPY as well as 2-nitrophenol as axial ligands.

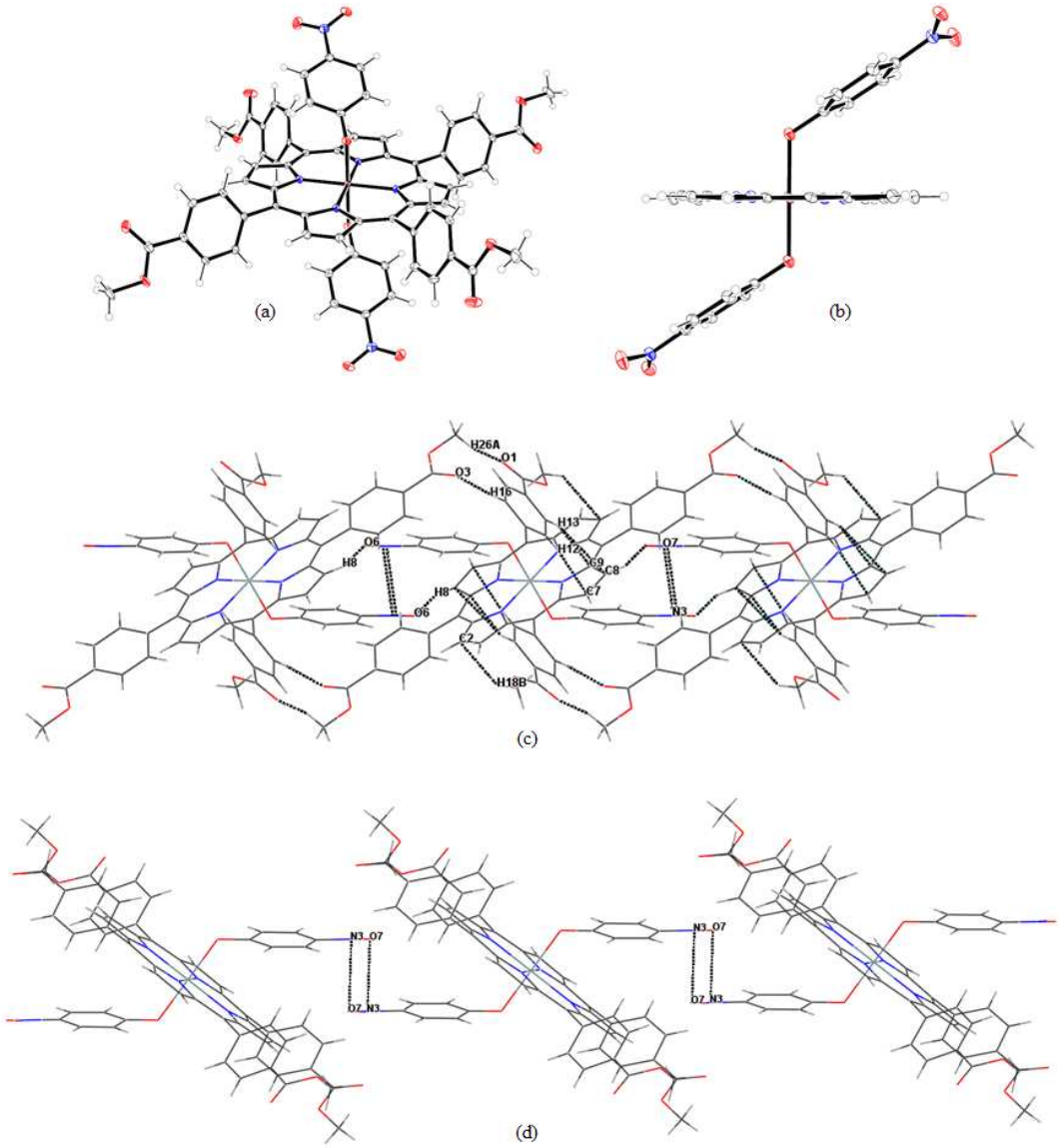

Fig. 4 ORTEP diagrams of **3** (a) top view and (b) side view (thermal ellipsoids shown at 40 % probability level; the aryl rings are omitted for clarity in side view of the molecule); (c) Molecular crystal packing diagram of **3** depicting various intermolecular interactions (viewed down 'a' axis); (d) One dimensional array of molecules involving complementary N···O bonding (viewed along 'ab' plane).

Table 3 The Sn^{IV}–O bond length in various tin(IV) porphyrins.

S. No	Sn^{IV}–O (Å)	Axial Ligand	Porphyrin
1	2.066	4-nitrophenolate	**3**
2	2.055	phenolate	TTP
3	2.083	4-nitrophenolate	TTP
4	2.062	phenolic BODIPY	TPP
5	2.070	2-nitrophenolate	TTP

Hirshfeld surface analysis

In order to further quantify the various intermolecular interactions in porphyrins $Sn^{IV}(Cl)_2T(4\text{-}CMP)P$ and **3**, Hirshfeld surfaces (HSs) and their associated fingerprint plots were calculated using *Crystal Explorer 3.1*.[17] The short and long close contacts can be visualized by color-coding, where the colour intensity indicates the relative strength of the interactions: red regions represent closer contacts and negative d_{norm} value; blue regions represent longer contacts and positive d_{norm} value; and white regions represent the distance of contacts is exactly the van der Waals separation and with a d_{norm} value of zero. The HSs of both the porphyrins $Sn^{IV}(Cl)_2T(4\text{-}CMP)P$ and **3** shows intense red spots due to the close O···H contacts whereas faint red spots are observed for N···H and C···H contacts for $Sn^{IV}(Cl)_2T(4\text{-}CMP)P$ and **3** respectively (Fig. 5). The 2D-fingerprint plot provides the decomposition of Hirshfeld surfaces into contribution of different intermolecular interactions present in crystal structure which features spike of various length and thickness.[34] A closer inspection at the FPs reveal that the major intermolecular interactions in both the complexes are mainly C···H [21.5 % in $Sn^{IV}(Cl)_2T(4\text{-}CMP)P$; 15.1 % in **3**], H···H [33.9 % in $Sn^{IV}(Cl)_2T(4\text{-}CMP)P$; 30.1 % in **3**] and O···H [16.5 % in $Sn^{IV}(Cl)_2T(4\text{-}CMP)P$; 27.6 % in **3**] contacts.

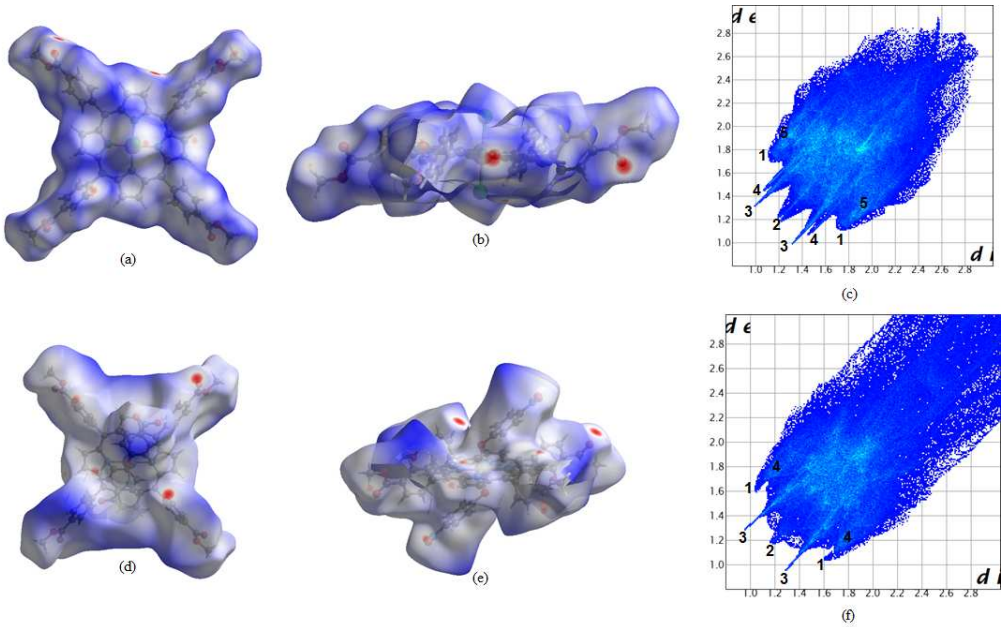

Fig. 5 Hirshfeld surfaces of porphyrins, **$Sn^{IV}(Cl)_2T(4\text{-}CMP)P$** and **3** (a, d) top view and (b, e) side view with d_{norm} mapped ranging from -0.28 (blue) to 3.49 (red); (c, f) Fingerprint plots of **$Sn^{IV}(Cl)_2T(4\text{-}CMP)P$** and **3** with d_i and d_e ranging from 1.0 to 2.8 Å. Close contacts are labeled as follows: C···H (1), H···H (2), O···H (3), N···H (4) and H···Cl (5).

Photodynamic inactivation of *C. albicans* using tin(IV) porphyrins

Agar well diffusion assay for determining the photodynamic growth inhibition of *C. albicans*

Earlier studies have shown the ability of *C. albicans* to exhibit multidrug resistance.[35] The photodynamic effect of porphyrins was assessed by performing zone of inhibition assay. It was found to be dependent on the photosensitization environment as the compounds which were illuminated with visible light showed maximum zone of inhibition as compared to the compounds which were left unilluminated. Fig. 6 indicates the drug concentration and its corresponding zone of inhibition in dark and light conditions. According to our study, compound **3** gave the maximum percentage inhibition in light in a concentration dependent manner *i.e.* around 24.4 % inhibition at 50 μM (30.9 μg/mL) concentration. Also, compounds **1**, **2** and the reference compound **R** showed a high percentage inhibition in a concentration dependant manner upon illumination. In dark, the zone of inhibition of the compounds is much lesser as compared to light illuminated. All the compounds showed a higher percentage of inhibition as compared to the standard antifungal drug fluconazole, which implicates the possible use of these compounds against multidrug resistant strains of *C. albicans*.

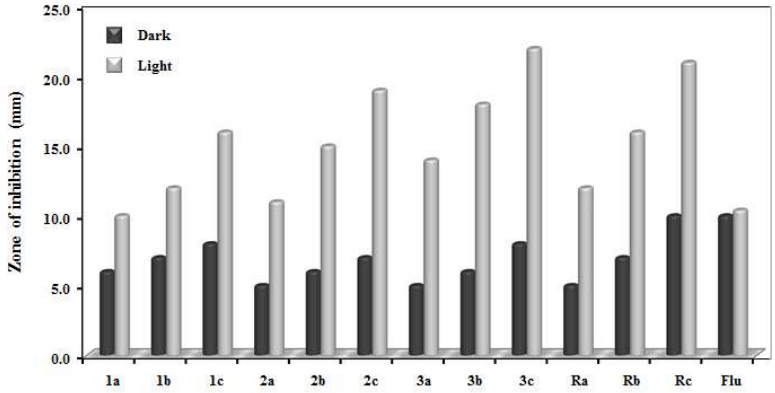

Fig. 6 Comparison of the percentage of inhibition by different compounds under light and dark conditions. Percentage of inhibition was found to increase with the increase in the concentrations of the compounds. a, b, and c refer to the concentrations 10, 25 and 50 μM respectively. All compounds showed higher percentage of inhibition as compared to the standard antifungal drug fluconazole.

Photodynamic inactivation of *C. albicans* in broth assay: Determination of IC_{50} and MIC values of porphyrins

Inhibition of growth of *C. albicans* cells in broth was studied under light and dark conditions. All the compounds show phototoxic effects in a time and concentration dependant manner. Porphyrins **1**, **2**, **3** and **R** inhibited the growth of *C. albicans* with an IC_{50} value of 14.7 μM,

9.1 μM, 9.0 μM and 9.4 μM respectively (Fig. 7). Interestingly, all the synthesized compounds exhibited lower IC_{50} values as compared to that of fluconazole (17.5 μM). Also, there was a significant difference between the percentage inhibition of porphyrins under light and dark conditions. Compounds, **1**–**3** exhibit a higher percentage of inhibition when exposed to light, however in dark the percentage of inhibition is significantly lower.

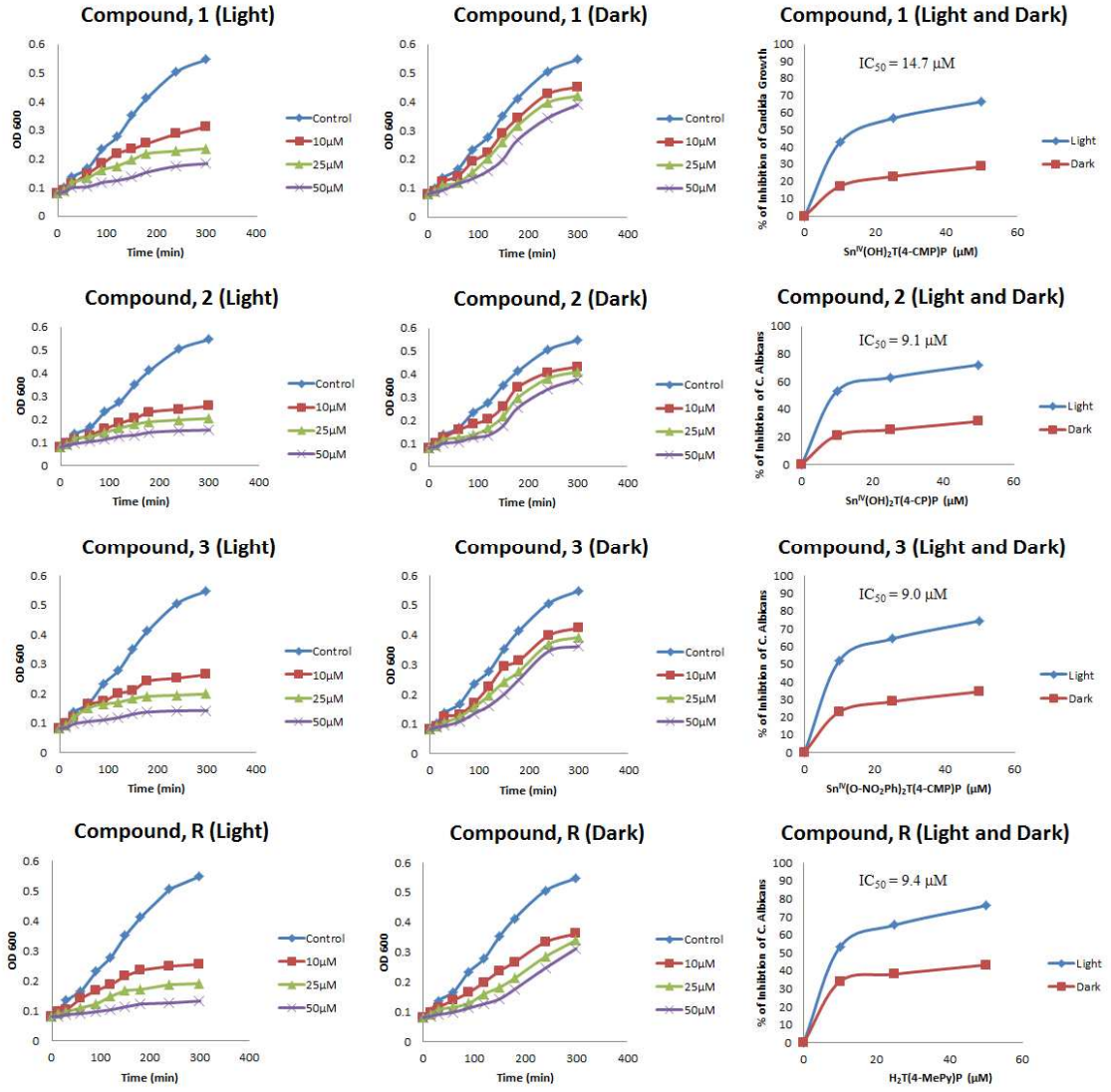

Fig. 7 *C. albicans* cells were grown in YPD broth medium supplemented with uridine, with varying concentrations of different porphyrins or DMSO (0.2 %). The study was performed in dark and light conditions. Growth curves for *C. albicans* cells in the absence (♦) and presence of 10 μM (▮), 25 μM (▲) and 50 μM (x) porphyrins are shown in the graph. The figure also shows the percentage inhibition of growth of *C. albicans* in the presence of different porphyrins in varying concentrations after 5 hrs of growth under light and dark conditions. The IC_{50} mentioned in the figures corresponds to the samples which were illuminated with light.

The concentration of compound at which lesser or no colonies observed was considered as the MIC.[36] Porphyrins at a concentration of 50 μM exhibits nearly complete inhibition of cell growth when exposed to light. Very few colonies (2-20) observed in the petri plates in which *C. albicans* cells treated with the compounds and exposed to light were plated. Importantly, compound **3** showed the least number of isolates. Comparatively more number of colonies (40-70) was observed when compound treated *C. albicans* cells, cultured under dark, were plated on the solid medium (Fig. 8). This shows that growth inhibitory effect of our compounds was maximum when the cells were exposed to light, explaining the photodynamic mode of action for our compounds.

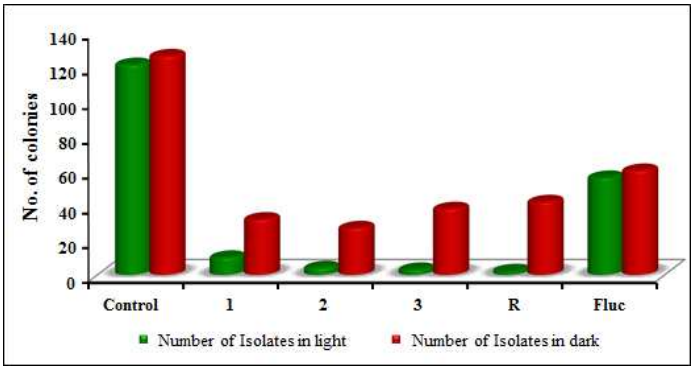

Fig. 8 Figure comparing the number of isolates obtained after plating the *C. albicans* cells, treated with 50 μM of porphyrins, cultured in light and dark conditions. Treated *C. albicans*, cultured in light, gave lesser number of colonies, upon plating. In general, *C. albicans* cells treated with different porphyrins gave lesser number of colonies upon plating as compared to the untreated cells.

Cellular uptake profiling of the porphyrins in *C. albicans* cells

The internalization profile indicates that the rate of internalization of all the compounds increased with time. It was found that compound **3** showed maximum internalization and compound **1**, the minimum internalization. These results are in compliance with those obtained from photodynamic inactivation experiments performed in this study in which compound **1** showed a higher IC_{50} value as compared to other compounds. In the light of the above observations, it is reasonable to suggest that the slow and inefficient internalization of compound **1** could be the reason for its least potency compared to other compounds under study (Fig. 9).

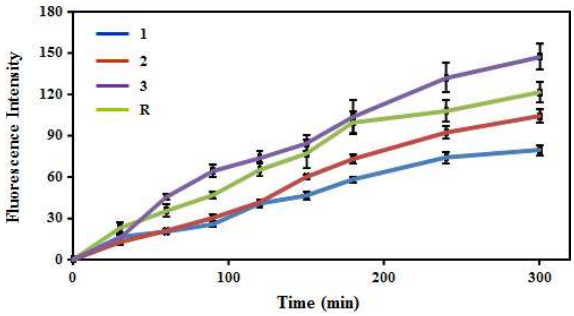

Fig. 9 The cellular uptake profiling study results reveals the slow intake of all porphyrins into the *Candida* cells. Compound **3** showed a better uptake profile than other compounds. Compound **1** showed relatively less internalisation as compared to the other compounds.

To study the internalization of porphyrins, a fluorescent microscopic analysis of *C. albicans* CAF4-2 cells was carried out by incubating the cells with tin(IV) porphyrins (Fig. 10). The cells exposed to all the three porphyrins exhibit fluorescence when excited using the green filter excitation, which confirms the internalisation of the compounds. Hoechst 33342 was used to stain the nucleus. The fluorescence of all the compounds was uniformly distributed throughout the cells, indicating their cytoplasmic localisation. These results also confirm that the cytotoxic effect on *C. albicans* was specifically due to the internalisation of the porphyrins.

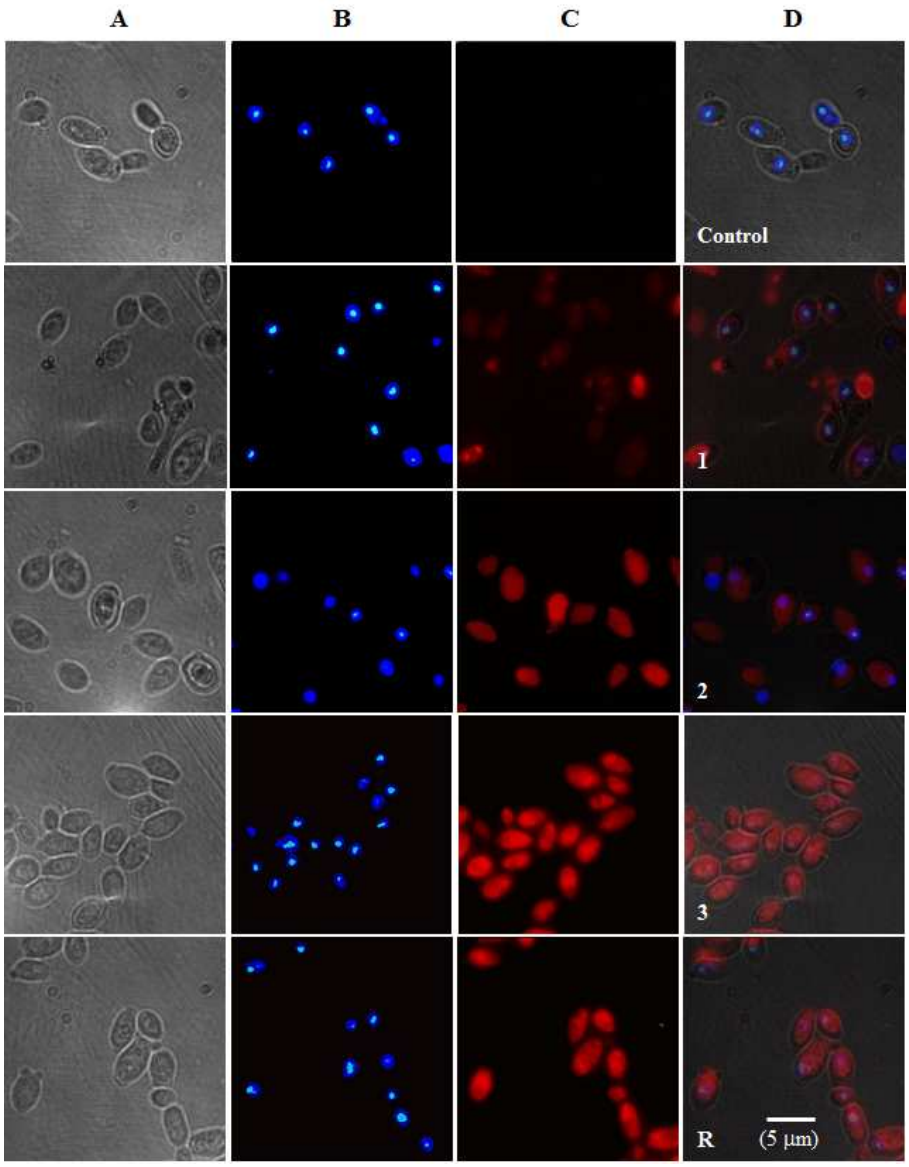

Fig. 10 Internalization of porphyrins in *C. albicans* CAF4-2. Cells were incubated with the solvent control (DMSO) or with different porphyrins, and were grown for 6 hrs and processed for microscopy as given in the materials and methods. (A) bright field image (B) Hoechst staining (C) porphyrin fluorescence (D) merged.

Confocal fluorescence microscopic studies

In order to confirm the internalisation of porphyrins in *C. albicans* cells, a progressive confocal microscopic analysis was performed. The cells were sliced optically through Z-axis with 0.8 µm depth. Compound **3** shows the best internalisation profile (Fig. 11). The *C. albicans* cells exposed to **3** were optically sliced. Red fluorescence of **3** increased progressively and reached maximum value at a depth of 2.4–4.8 µm (Fig 11 E-G) within the cells. Red fluorescence is negligible on the upper and lower sections of the cells (Fig 11 A, B

and J), showing that there is no or less binding of the compound with the cell membrane. In all the cases, red fluorescence increases as the cells were sliced deeper, confirming the internalization and cytoplasmic localization of the compounds. All the other compounds showed proper internalisation (data not shown). This data is in support with the results obtained from fluorescent wide field imaging.

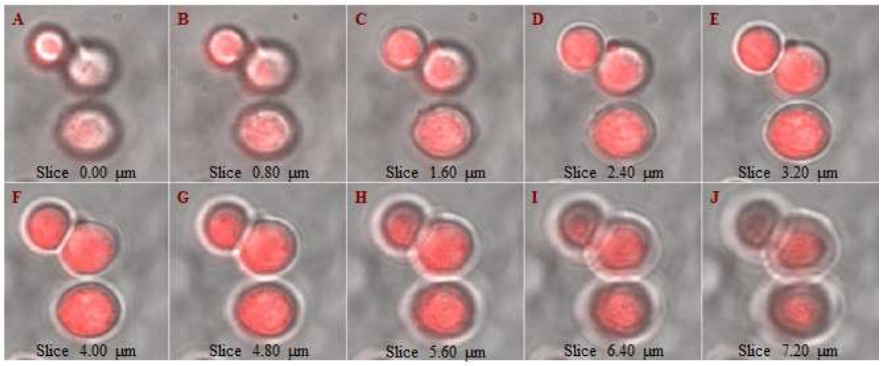

Fig. 11 Internalisation of compound **3** by progressive confocal optical slicing of *C. albicans*. Images were obtained by merging bright field and fluorescent images. A-J: As the 0.8 µm slices progress deeper within the cells, the intensity of red fluorescence increased and reached a maximum at the middle portion, indicating efficient compound internalization i.e. within the cell's cytoplasm.

It is well documented that photosensitizers like porphyrins were known to interfere with the mitochondrial membrane potential and release the inner mitochondrial membrane enzymes like cytochrome c and activate cell death pathways.[37] Because of the bright cytoplasmic staining, we were not able to clearly differentiate the internalization of the synthesized porphyrins to the other cellular organelles like mitochondria or vacuoles which is also quite possible.

Photogeneration of singlet oxygen

The photodynamic inactivation of *C. albicans* could be through the generation of singlet oxygen species within the cells. This can be visualized using 1,3-diphenylisobenzofuran (DPBF) which was able to capture the $^1O_2$ generated by the porphyrins.[2c,25] The relationship between the change in absorbance by DPBF and irradiation time reflects the $^1O_2$ yield of the compounds. The absorbance of DPBF at 410 nm decreased in the presence of porphyrin with increasing irradiation time and from the slope of the line, the relative rate of $^1O_2$ generation was compared. Higher the line slopes, higher the $^1O_2$ yield. From the plot, the order of $^1O_2$

generation rate was found to be **3** > **2** > **1** > **R** > **H_2TPP** (Fig. 12). The results are in good agreement with the antifungal assays and fluorescence microscopic results.

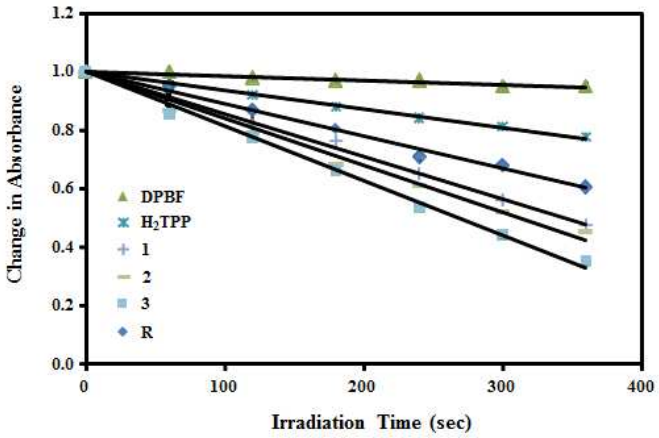

Fig. 12 Plot of change in absorbance of DPBF *vs.* irradiation time in the presence of porphyrins.

DFT calculations for HOMO-LUMO gap in porphyrins

In order to understand more about the electronic transitions, we have performed DFT calculations at the BP86/def2-SVP level of theory[38] using Gaussian 09[39] program package for compounds using their crystallographic information files (CIF) obtained from the single crystal X-ray diffraction studies. For comparison, we have optimized the structures of H_2TPP and H_2T(4-NMP)P. The highest occupied molecular orbital (HOMO) and lowest unoccupied molecular orbital (LUMO) of free base porphyrins, H_2TPP, H_2T(4-NMP)P and tin(IV) porphyrins, $Sn^{IV}(Cl)_2$T(4-CMP)P, **1** and **3** are shown in the Fig. 13. For free base porphyrins, the HOMO and LUMO is a typical π-type orbital on the porphyrin core. Hence, the electronic transition is a well-known $\pi \rightarrow \pi^*$ type transition upon excitation. In the case of $Sn^{IV}(Cl)_2$T(4-CMP)P, the HOMO is mainly based on the porphyrin core and axial ligand chlorine has lesser contribution. Here, the HOMO-1 is porphyrin based orbital and the HOMO-2 and HOMO-3 is concentrated on the axial ligand (Fig. S9). For **1**, the HOMO doesn't have any contribution from the axial ligand, whereas the HOMO-1, which is slightly lesser in energy than HOMO (ΔE = 0.05 eV) have more contribution from the hydroxyl moiety (Fig. S10). For **3**, the HOMO has major contribution from 4-nitrophenolate moiety and also the underlying orbitals, HOMO-1 and HOMO-2 has contribution from the axial ligand (Fig. S11). In all the above structures the LUMO is a π based orbital on the porphyrin core.

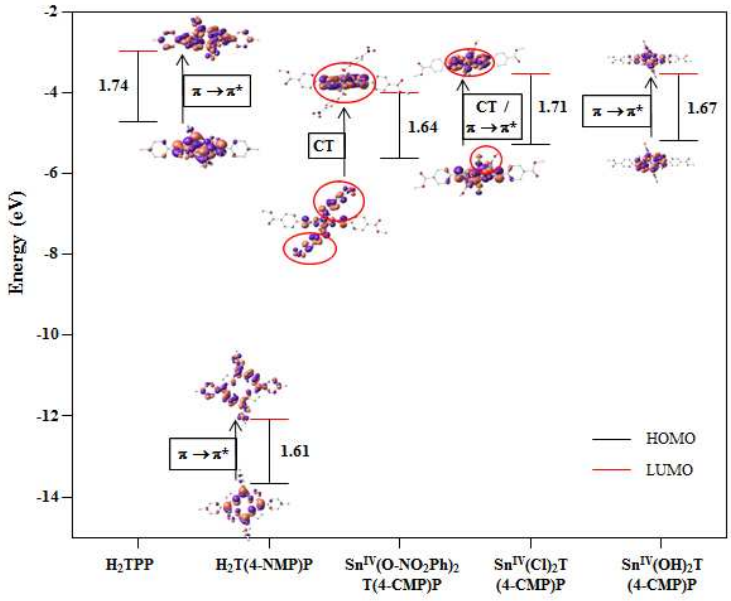

Fig. 13 Orbital energies (in eV) at the BP86/def2-SVP level of theory for the compounds. The nature of highest occupied molecular orbital (HOMO) and lowest occupied molecular orbital (LUMO) and the HOMO-LUMO gap of the compounds are shown.

On analyzing the electronic transitions based on the nature of orbitals in tin(IV) porphyrins, there is a charge transfer (CT) from chlorine atom, hydroxyl and 4-nitrophenolate group to the porphyrin core in $Sn^{IV}(Cl)_2T(4\text{-CMP})P$, **1** and **3** respectively. Since chlorine has less contribution in the HOMO of $Sn^{IV}(Cl)_2T(4\text{-CMP})P$, $\pi \rightarrow \pi^*$ is more favorable and the extend of CT will be less since the orbitals corresponding to CT (HOMO-2 and HOMO-3) (Fig. S9) is stabilized much on comparing with HOMO. Upon photon excitation, both $\pi \rightarrow \pi^*$ and CT transition are possible in **1**, which are energetically more favorable because the HOMO has a π-type character and the HOMO-1 has contribution from the hydroxyl fragment, $\Delta E_{[HOMO-(HOMO-1)]} = 0.05$ eV. However, **3** shows the most prominent charge transfer from the 4-nitrophenolate to porphyrin core which is the cause for the intersystem crossing (ISC), in turn resulting in the higher population of lower energy triplet state.[40] Our experimental results which also correlates with the theoretical observations that **3** shows more phototoxicity which can be attributed to more CT which in turn results in the generation of more singlet oxygen. Hence, the enhanced phototoxicity of **3** is in concordance with the DFT calculations. The results of all the above studies show that the newly synthesized porphyrins **2** and **3** possibly the better candidates for treating *C. albicans* infections.

Conclusions

In summary, high valent tin(IV) porphyrins, **1**–**3** were synthesized, characterized and their photophysical properties were studied. X-ray crystal structure determination of porphyrins $Sn^{IV}(Cl)_2T(4\text{-}CMP)P$ and **3** were achieved successfully and the result shows that there is π–π interaction between the porphyrin plane and 4-nitrophenyl system in **3** due to their close proximity. We also explored the potential applications of these newly synthesized tin(IV) porphyrins towards photodynamic antimicrobial chemotherapy (PACT) in *C. albicans*. The light and dark experiments carried out in agar plates and broth media supports the photodynamic inactivation of *C. albicans*. Porphyrins, **1**–**3** showed lower IC_{50} values than the standard drug fluconazole. Also, **2** and **3** possess high cellular penetration and cytoplasmic binding compared to **1**. Wide field and confocal fluorescence microscopic experiments are evident for porphyrin internalisation throughout the cytoplasm which is the main reason behind the induced phototoxicity. The higher activity of **3** is further supported by DFT calculations which reveal the most prominent charge transfer from 4-nitrophenolate to porphyrin core. This charge transfer increases the population of lower energy triplet state leading to the generation of more singlet oxygen. To conclude, porphyrins **1–3** exhibited significant antimicrobial activities, and especially **2** and **3** could be developed as new antifungal agents for treating *C. albicans* infections.

Acknowledgements

The Department of Science and Technology (DST), New Delhi is gratefully acknowledged for the financial support to SS (SR/WOS-A/CS-146/2011) and CA (SB/EMEQ-016/2013). We express our sincere thanks to Prof. T. N. Guru Row and Mr. Vijith Shetty for one of the single crystal data collections. Authors are thankful to Dr. Babu Varghese, SAIF, IIT Madras for another single crystal data collection, structure solution and refinement. We acknowledge Ms. Indu, P, Ms. Rojisha, V. C and Dr. P. Parameswaran, Theoretical and Computational Chemistry Laboratory, Department of Chemistry, NIT Calicut for the DFT calculations. We would like to thank Prof. I. Ibnusaud for providing ^1H NMR facility at Institute for Intensive Research in Basic Sciences (IIRBS), MG University, Kottayam. We thank Ms. Agisha and Dr. R Suseela Bhai for providing wide field microscope facility at Indian Council of Agricultural Research (ICAR) – Indian Institute of Spices Research (IISR), Calicut. Our thanks due to Mr. Vimal, G and Dr. Santhosh for providing Fluoromax-4 fluorescence

spectroscopy facility at School of Pure and Applied Physics, MG University, Kottayam. We also extend our thanks to Dr. Anilkumar P. R. for providing confocal microscopy facility at Tissue culture laboratory, Sree Chitra Tirunal Institute for Medical Sciences and Technology (SCTIMST), Trivandrum.

Note and References

[a]Bioinorganic Materials Research Laboratory, Department of Chemistry, National Institute of Technology Calicut, Kozhikode, Kerala, India – 673 601; E-mail address: arunkumarc@nitc.ac.in (C. Arunkumar)

[b]School of Biotechnology, National Institute of Technology Calicut, Kozhikode, Kerala, India – 673 601; E-mail address: rathin@nitc.ac.in (K. Rathinasamy)

[†]Electronic supporting information: Additional figures, ^{1}H NMR and mass spectra.

References

1. M. Wainwright, *J. Antimicrob. Chemother.,* 1998, **42**, 13.
2. (a) E. D. Sternberg, D. Dolphin and C. Bruckner, *Tetrahedron.*, 1998, **54**, 4151; (b) L. M. Giroldo, M. P. Felipe, M. A. de Oliveira, E. Munin, L. Procopio Alves and M. S. Costa, *Laser. Med. Sci.,* 2009, **24**, 109; (c) S. C. Karunakaran, P. S. Babu, B. Madhuri, B. Marydasan, A. K. Paul, A. S. Nair, K. S. Rao, A. Srinivasan, T. K. Chandrashekar, Ch. M. Rao, R. Pillai and D. Ramaiah, *ACS Chem. Biol.,* 2012, **8**, 127.
3. (a) M. M. Gois, C. Kurachi, E. J. B. Santana, E. G. O. Mima, D. M. P. Spolidório, J. E. P. Pelino and V. S. Bagnato, *Laser. Med. Sci.,* 2010, **25**, 391; (b) D. A. Caminos, M. B. Spesia, P. Pons and E. N. Durantini, *Photochem. Photobiol. Sci.,* 2008, **7**, 1071.
4. (a) M. J. McCullough, B. C. Ross and P. C. Reade, *Int. J. Oral Maxillofac Surg.,* 1996, **25**, 136; (b) G. Molero, R. D. Orejas, F. N. García, L. Monteoliva, J. Pla, C. Gil, M.S. – Pérez and C. Nombela, *Internatl. Microbiol.,* 1998, **1**, 95.
5. C. Onyewu, J. R. Blankenship, M. D. Poeta and J. Heitman, *Antimicrob. Agents Chemother.,* 2003, **47**, 956.
6. (a) D. Sanglard, K. Kuchler, F. Ischer, J. L. Pagani, M. Monod and J. Bille, *Antimicrob. Agents Chemother.,* 1995, **39**, 2378; (b) S. A. Flowers, B. Colon, S. G. Whaley, M. A. Schuler and P. D. Rogers, *Antimicrob. Agents Chemother.,* 2015, **59**, 450
7. E. S. Nyman and P. H. Hynninen, *J. Photochem. Photobiol. B.*, 2004, **73**, 1.

8. (a) K. P. Ghiggino, N. K. Giri, J. Hanrieder, J. D. Martell, J. Müller, M. F. Paige, B. Robotham, J. Szmytkowski and R. P. Steer, *J. Phy. Chem. A.,* 2013, **117**, 7833; (b) S. Dey, P. Mondal and S. P. Rath, *New J. Chem.,* 2015, **39**, 4100.
9. (a) D. P. Arnold and J. Blok, *Coord. Chem. Rev.,* 2004, **248**, 299; (b) V. S. Shetti, Y. Pareek and M. Ravikanth, *Coord. Chem. Rev.,* 2012, **256**, 2816.
10. (a) B. W. Pogue, R. W. Redmond, N. Trivedi and T. Hasan, *Photochem. Photobiol.,* 1998, **68**, 809; (b) D. E. J. G. J. Dolmans, D. Fukumura and R. K. Jain, *Nat. Rev. Cancer.,* 2003, **3**, 380; (c) M. R. Detty, S. L. Gibson and S. J. Wagner, *J. Med. Chem.,* 2004, **47**, 3897; (d) W. M. Sharman, C. M. Allen and J.E. Van Lier, *Drug Discov. Today.,* 1999, **4**, 507.
11. D. D. Perrin and W. L. F. Armarego, Purification of Organic Solvents, Pergamon Press, Oxford, 1988.
12. J. S. Lindsey, I. C. Schreiman, H. C. Hsu, P. C. Kearney and A. M. Marguerettaz, *J. Org. Chem.,* 1987, **52**, 827.
13. J. S. Lindsey and R. W. Wagner, *J. Org. Chem.,* 1989, **54**, 828.
14. (a) D. P. Arnold, *J. Chem. Edn.,* 1988, **65**, 1111; (b) M. J Crossley, P. Thordarson and R. A-S. Wu, *J. Chem. Soc. Perkin Trans. 1.,* 2001, 2294; (c) P. Bhyrappa, C. Arunkumar and J. J. Vittal, *J. Chem. Sci.,* 2005, **117**, 139.
15. (a) A. G. Altomare, G. Cascarano, C. Giacovazzo and A. Gualardi, *J. Appl. Crystallogr.,* 1993, **26**, 343; (b) L. J. Farrugia, *J. Appl. Crystallogr.,* 1999, **32**, 837.
16. G. M. Sheldrick, SHELXL97; University of Goettingen: Goettingen, Germany, 1997.
17. (a) S. K. Wolff, D. J. Grimwood, J. J. McKinnon, M. J. Turner, D. Jayatilaka and M. A. Spackman, Crystal Explorer 3.1 (2013), University of Western Australia, Crawley, Western Australia, 2005-2013; http://hirshfeldsurface.net/CrystalExplorer; (b) M. A. Spackman and D. Jayatilaka, *CrystEngComm.,* 2009, **11**, 19.
18. D. M. Hampsey, G. Das and F. Sherman, *J. Biol. Chem.,* 1986, **261**, 3259.
19. W. A. Fonzi and M. Y. Irwin, *Genetics.,* 1993, **134**, 717.
20. J. V. Bennett, J. L. Brodie, E. J. Benner and W. M. M. Kirby, *Appl. Microbiol.,* 1966, **14**, 170. (b) S. S. Magaldi, C. Mata-Essayag, H. De Capriles, C. Perez, M. T. Colella, C. Olaizola and Y. Ontiveros. *Int. J. Infect. Dis.,* 2004, **8**, 39.
21. D. Rai, J. K. Singh, N. Roy and D. Panda, *Biochem. J.,* 2008, **410**, 147.
22. S. Makhseed, M. Machacek, W. Alfadly, A. Tuhl, M. Vinodh, T. Simunek, V. Novakova, P. Kubat, E. Rudolf and P. Zimcik, *Chem. Commun.,* 2013, **49**, 11149.

23. (a) P. Appadurai and K. Rathinasamy, *Toxicol. Lett.,* 2014, **225**, 66; (b) D. Suresh, M. S. Balakrishna, K. Rathinasamy, D. Panda and S. M. Mobin, *Dalton Trans.,* 2008, 2812; (c) S. A. G. Lambrechts, M. C. G. Aalders and J. Van Marle, *Antimicrob. Agents Chemother.,* 2005, **49**, 2026; (d) J. M. Bliss, C. E. Bigelow, T. H. Foster and C. G. Haidaris, *Antimicrob. Agents Chemother.,* 2004, **48**, 2000; (e) S. Oriel and Y. Nitzan. *Photochem. Photobiol.,* 2012, **88**, 604.
24. K. Rathinasamy, B. Jindal, J. Asthana, P. Singh, P. V. Balaji and D. Panda, *BMC Cancer.,* 2010, **10**, 213.
25. M. O. L. Lourenço, B. A. Iglesias, M. R. P. Pereira, H. Girão, R. Fernandes, M. G. P. M. S. Neves, J. A. S Cavaleiro, and J. P. C. Tomé. *Dalton Trans.,* 2015, **44**, 530.
26. (a) D. R. Reddy and B. G. Maiya, *J. Porphyrins Phthalocyanines.,* 2002, **6**, 3; (b) A. A. Kumar, L. Giribabu, D. R. Reddy and B. G. Maiya. *Inorg. Chem.,* 2001, **40**, 6757.
27. (a) P. G. Seybold and M. Gouterman, *J. Mol. Spectrosc.,* 1969, **31**, 1; (b) O. Ohno, Y. Kaizu and H. Kobayashi, *J. Chem. Phys.,* 1985, **82**, 1779.
28. T. Zoltan, F. Vargas, V. Lopez, V. Chavez, C. Rivas and A. H. Ramirez, *Spectrochim. Acta Part A Mol. Biomol. Spectrosc.,* 2015, **135**, 747.
29. H. J. Kim, K.-M. Park, T. K. Ahn, S. K. Kim, K. S. Kim, D. Kim and H.-J. Kim, *Chem. Commun.,* 2004, 2594.
30. N. Venkatramaiah, B. Ramakrishna, A. R. Kumar, N. Veeraiah and R. Venkatesan, *J. Alloys Compd.,* 2012, **513**, 318.
31. S. J. Langford, A. P. Marcia, K. J. Lee, K. J. Macfarlane and J. A. Weigold, *J. Incl. Phenom. Macrocycl. Chem.,* 2001, **41**, 135.
32. T. Lazarides, S. Kuhri, G. Charalambidis, M. K. Panda, D. M. Guldi and A. G. Coutsolelos, *Inorg. Chem.,* 2012, **51**, 4193.
33. G. D. Fallon, M. A. P. Lee, S. J. Langford and P. J. Nichols, *Org. Lett.,* 2002, **4**, 1895.
34. (a) F. R. Kooriyaden, S. Sujatha, B. Varghese and C. Arunkumar, *J. Fluor. Chem.,* 2015, **170**, 10; (b) R. Soman, S. Sujatha and C. Arunkumar, *J. Fluor. Chem.,* 2014, **163**, 16.
35. (a) L. Millon, A. Manteaux, G. Reboux, C. Drobacheff, M. Monod, T. Barale and Y. M. Briand, *J. Clin. Microbiol.,* 1994, **32**, 1115; (b) R. Franz, S. L. Kelly, D. C. Lamb, D. E. Kelly, M. Ruhnke and J. Morschhäuser, *Antimicrob. Agents Chemother.,* 1998, **42**, 3065.
36. T. Beuria, P. Singh, A. Surolia and D. Panda. *Biochem. J.,* 2009, **423**, 61.

37. (a) D. Kessel and Y. Luo, *Cell Death Differ.*, 1999, **6**, 28; (b) R. Hilf, *J. Bioenerg. Biomembr.*, 2007, **39**, 85; (c) P. Mroz, A. Yoroslavsky, G. B. Kharkwal and M. R. Hamblin, *Cancers*, 2011, **3**, 2516.
38. (a) A. D. Becke, *Physical Review A.,* 1988, **38**, 3098; (b) F. Weigend and R. Ahlrichs, *Phy. Chem. Chem. Phy.,* 2005, **18**, 3297.
39. M. J. Frisch, G. W. Trucks, H. B. Schlegel, G. E. Scuseria, M. A. Robb, J. R. Cheeseman, G. Scalmani, V. Barone, B. Mennucci, G. A. Petersson, H. Nakatsuji, M. Caricato, X. Li, H. P. Hratchian, F. Izmaylov, J. Bloino, G. Zheng, J. L. Sonnenberg, M. Hada, M. Ehara, K. Toyota, R. Fukuda, J. Hasegawa, M. Ishida, T. Nakajima, Y. Honda, O. Kitao, H. Nakai, T. Vreven, J. A. Montgomery, Jr., J. E. Peralta, F. Ogliaro, M. Bearpark, J. J. Heyd, E. Brothers, K. N. Kudin, V. N. Staroverov, T. Keith, R. Kobayashi, J. Normand, K. Raghavachari, A. Rendell, J. C. Burant, S. S. Iyengar, J. Tomasi, M. Cossi, N. Rega, J. M. Millam, M. Klene, J. E. Knox, J. B. Cross, V. Bakken, C. Adamo, J. Jaramillo, R. Gomperts, R. E. Stratmann, O. Yazyev, A. J. Austin, R. Cammi, C. Pomelli, J. W. Ochterski, R. L. Martin, K. Morokuma, V. G. Zakrzewski, G. A. Voth, P. Salvador, J. J. Dannenberg, S. Dapprich, A. D. Daniels, O. Farkas, J. B. Foresman, J. V. Ortiz, J. Cioslowski and D. J. Fox, Gaussian 09 (Revision B.01), Gaussian Inc., Wallingford CT, 2010.
40. S. Kolemen, M. Işık, G. M. Kim, D. Kim, H. Geng, M. Buyuktemiz, T. Karatas, X.-F. Zhang, Y. Dede, J. Yoon and E. U. Akkaya, *Angew. Chem. Int. Ed.,* 2015, **54**, 5340.